SUPERDIMENSIONAL METAMATERIAL RESONATORS FROM SUB-RIEMANNIAN GEOMETRY[*]

ALLAN GREENLEAF[†], HENRIK KETTUNEN[‡], YAROSLAV KURYLEV[§],
MATTI LASSAS[‡], AND GUNTHER UHLMANN[¶]

Abstract. We introduce a fundamentally new method for the design of metamaterial arrays. These behave superdimensionally, exhibiting a higher local density of resonant frequencies, giant focusing of rays, and stronger concentration of waves than expected from the physical dimension. This *sub-Riemannian optics* allows planar designs to function effectively as 3- or higher-dimensional media, and bulk material as dimension 4 or higher. Valid for any waves modeled by the Helmholtz equation, including scalar optics and acoustics, and with properties derived from the behavior of waves in sub-Riemannian geometry, these arrays can be assembled from nonresonant metamaterial cells and are potentially broadband. Possible applications include antenna design and energy harvesting.

Key words. transformation optics, metamaterials, sub-Riemannian geometry

AMS subject classifications. 35J70, 35P05, 78A48

DOI. 10.1137/17M1130964

1. Introduction. The advent of transformation optics has resulted in numerous theoretical designs allowing extreme manipulation of waves, including cloaks [5, 16, 6, 7, 27, 28, 35, 38, 42], field rotators [13], electromagnetic wormholes [19, 22], and illusion optics [33], among many others; see also [21, 25]. The ongoing development of metamaterials has allowed some of these plans to be implemented in at least a reasonable approximation to the theoretically perfect ideal [46, 40]. Since a variety of physical waves may be modeled by one partial differential equation, a single theoretical transformation optics design may in principle be implemented for a number of distinct wave phenomena. Thus, a Helmholtz equation design can be applied to scalar optics [38], electromagnetism in cylindrical geometry, acoustics [15, 26, 34], small amplitude water waves [14], and even matter waves in quantum mechanics [20, 52, 23, 24]. The possibility of realizing such devices then depends on the ability to fabricate suitable metamaterial (MM) cells for the wave type and wavelengths of interest and the feasibility of assembling these into the array required by the design. The mathematical theory of the subwavelength resonators, such as plasmonic nanoparticles, Helmholtz resonators, and Minnaert bubbles, that could be used as the

[†]Department of Mathematics, University of Rochester, Rochester, NY 14627 (allan@math.rochester.edu).

[‡]Department of Mathematics, University of Helsinki, FIN-00014 Helsinki, Finland (Henrik.Kettunen@gmail.com, Matti.Lassas@helsinki.fi).

[§]Department of Mathematical Sciences, University College London, London, WC1E 6BT, UK (y.kurylev@ucl.ac.uk).

[¶]Department of Mathematics, University of Washington, Seattle, WA 98195 (gunther@math.washington.edu).

building blocks of metamaterials, has been recently investigated in [1, 2, 3, 4].

In this paper, we propose a new method for designing MM arrays, modeled by Helmholtz-type equations, where some eigenvalues of the material parameter tensor may be zero. We refer to this as *sub-Riemannian optics* (SRO), since it is based on the behavior of spectral asymptotics, Green's functions, and rays for sub-Riemannian (SR) geometries [48, 43]. We introduce SRO by examining some axially symmetric designs, both planar and bulk, analysis of which is based on the quantum harmonic oscillator in dimension 1 (1D) and its degenerate variants. The resulting novel properties hold for any wave phenomena modeled by a Helmholtz equation; the designs most easily realizable using currently available metamaterials would be for acoustics and polarized electromagnetism (EM).

SRO media are notable for their *superdimensionality*: power laws for various physical properties mimic those of a larger dimension than the physical dimension. We focus on two such properties: (i) very high density of resonant frequencies over finite but large frequency bands, a density much larger than that dictated by Weyl's law [49] for conventional media (Figure 1), and (ii) giant focusing of rays and concentration of waves (Figure 2).
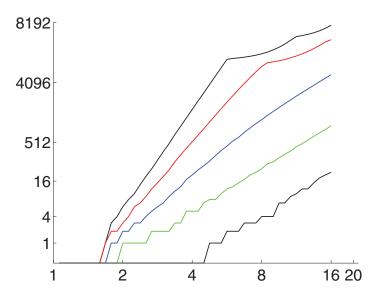

FIG. 1. *Superdimensional density of resonant frequencies. The figure shows the logarithms of the eigenfrequency count functions* $\log N(\omega)$ *(on the vertical axis) as a function of* $\log \omega$ *(on the horizontal axis) for five 2-dimensional (2D) media: The lower black line is the eigenfrequency count function* $N(\omega)$ *for homogeneous material (r = 0), and the other curves are the functions* $N(\omega)$ *for the approximate SRO resonators (9) satisfying the Dirichlet boundary condition (BC) in rectangle R, with r = 4 (upper black line), r = 3 (red), r = 2 (blue), and r = 1 (green). (Approximation parameter a = 0.1 for all.) The various* $N(\omega)$ *display superdimensional behavior for* $0 < \omega < \Omega_{r,a} = \sqrt{c_r}a^{-1}$, *with high density of frequencies near* $\Omega_{r,a}$, *and the usual 2D growth in the high frequency regime* $\omega > \Omega_{r,a}$.

SRO media are highly inhomogeneous and anisotropic. Ideal designs use smoothly spatially varying and anisotropic material parameters with infinitely slow wave propagation at some points and in some directions. Recall that the metamaterials required for many transformation optics designs involve parameters at or close to zero and
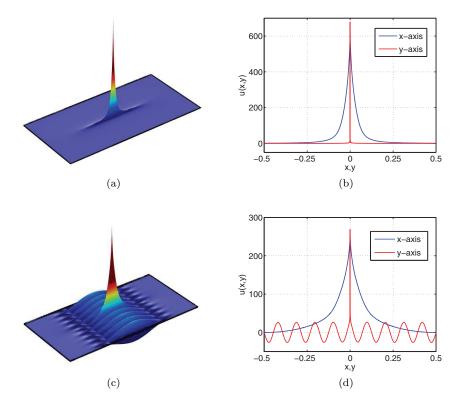
FIG. 2. *Superdimensional wave concentration. Green's functions for $r = 2$ with pole at $\mathbf{p} = (0,0)$. Frequency $\omega = 0$: as a graph showing strongly anisotropic peak at pole* (a) *and values along x and y axes* (b). (c), (d) *exhibit $\omega = 4$ in same manner.*

are inherently dispersive (for EM), or have negative index and are lossy. In contrast, SRO designs, since they do not require superluminal phase velocity, are potentially broadband. We define and analyze both ideal and approximate SRO designs, the latter being more physically realistic and implementable (at the price of a quantifiable degradation in performance), yet retaining the characteristic features of ideal SRO.

Transformation optics designs which strongly concentrate EM waves have also been obtained previously by [39]. However, the analysis and geometry which are the basis for SRO and produce superdimensionality for several distinct phenomena make it a fundamentally new approach. Devices with anomalous resonant frequency distributions have also been described previously, e.g., fractal antennas [51] and wire media [36, 47]. However, in contrast to the former, SRO devices have smooth material parameters and are not self-similar, while wire media exploit axial symmetries different from those of SRO and are not related to sub-Riemannian geometry.

MM arrays approximately implementing SRO designs can be realized using simple, nonresonant MM cells (meta-atoms) composed of rectangles of low speed material on a square substrate of roughly unit speed material, with increasing vertical fill ratios as $x \to 0$. Since the MM atoms used are nonresonant, standard effective medium approximations used to derive the effective parameters should be valid over a broad band. See Figure 3, the effective medium theory in section 4, and a discussion of possible implementations in section 6.
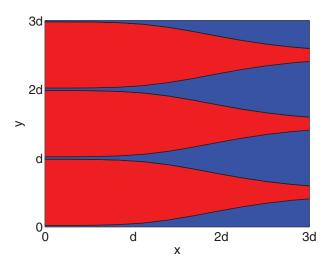
FIG. 3. *SRO metamaterial. Schematic top view of a 2D SRO medium for electromagnetism at subwavelength scale d near the axis $x = 0$. MM cells are grouped to form x-directed strips of varying width $w(x)$ and high permittivity (red), embedded in background material with relative permittivity $\varepsilon_r = 1$ (blue). The inhomogeneity in x of the strip widths is crucial for the various superdimensional properties of the material. Color is available online only.*

For simplicity, the models we describe are homogeneous parallel to the axis of degeneracy, but that symmetry is not required for the novel properties of SRO materials: property (i) above results from the hypoelliptic nature of the PDE governing wave propagation, and (ii) is a consequence of the focusing behavior of the rays in the high frequency limit, controlled by the associated sub-Riemannian geometry [48, 43]. This opens up a fundamentally new and flexible approach to the design of MM arrays.

2. Ideal planar SRO. We start by considering model SRO designs based on a family of quantum oscillators in 1D. Fix an integer $r \geq 1$ and consider a Helmholtz equation in 2D at frequency $\omega > 0$ for a wave $u(\mathbf{p})$ on a rectangle $R = \{\mathbf{p} = (x, y) : |x| \leq 1, -\frac{1}{2} \leq y \leq \frac{1}{2}\}$,

$$(1) \qquad \left(\left(\partial_x^2 + x^{2r} \partial_y^2 \right) + \omega^2 \right) u(\mathbf{p}) = 0.$$

Elliptic for $x \neq 0$ but degenerate on the axis $x = 0$, (1) was first studied by Grushin [29] (for $\omega = 0$). We impose the Dirichlet BC on the boundary of R, $u(x, y) = 0$ for $|x| = 1$ or $|y| = \frac{1}{2}$, representing, e.g., a sound-soft BC in acoustics, but similar results hold for a Neumann or mixed BC.

2.1. Superdimensionality of frequency count. For waves propagating in homogeneous, isotropic material in d dimensions, modeled by $(\nabla^2 + \omega^2)u = 0$, Weyl's law states that the number of resonant frequencies ω_j grows as $N(\omega) := \#\{\omega_j : \omega_j \leq \omega\} \sim c \cdot \omega^d$ [49]. Here and below, we denote $N(\omega) \sim c \cdot \omega^{d_1}$ when $N(\omega) = c \cdot \omega^{d_1} + O(\omega^{d_2})$, as $\omega \to \infty$, with some $d_2 < d_1$. This also holds for general *nondegenerate* media, for which the mass-density or analogous tensor is nonsingular and thus the wave is modeled by an *elliptic* PDE. There is also a mathematical literature on spectral asymptotics for *degenerate*-elliptic equations such as (1), e.g., [41], but here we derive them directly from eigenvalues and eigenfunctions of quantum oscillators, harmonic for $r = 1$ and degenerate for $r \geq 2$.

For solutions to (1) of the form

$$u(x,y) = \psi_n(x) \sin\left(n\pi\left(y + \frac{1}{2}\right)\right), \quad n = 1, 2, \ldots,$$

on $|x| \leq 1$ the ψ_n satisfy

$$(2) \qquad L_n\psi_n := \left(\frac{d^2}{dx^2} - \pi^2 n^2 x^{2r}\right)\psi_n = -\omega^2\psi_n, \qquad \psi_n(\pm 1) = 0.$$

For now, omit the BC and consider the same equation on the entire real line. The operator $L := d^2/dz^2 - z^{2r}$ has eigenvalues $\{-\lambda_l\}_{l=1}^\infty$ and L^2-normalized eigenfunctions $\{\phi_l\}_{l=1}^\infty$. For $r = 1$, $\lambda_l = 2l + 1$ and the ϕ_l are the Hermite functions [49]. For $r \geq 2$, the λ_l and ϕ_l are less explicit, but it is known that $\lambda_l \sim c_r l^{\frac{2r}{r+1}}$ and

$$|\phi_l(z)| \leq c_{l,\epsilon}\exp\left(-\frac{|z|^{r+1}}{r+1}(1-\epsilon)\right)$$

for any $\epsilon > 0$; see [37, 50]. Letting

$$\widetilde{\psi}_{l,n}(x) = (\pi n)^{\frac{1}{2(r+1)}}\phi_l\left((\pi n)^{\frac{1}{r+1}}x\right), \qquad |x| \leq 1,$$

$\widetilde{\psi}_{l,n}$ satisfies the ODE in (2) with $\omega = \widetilde{\omega}_{l,n} := (\pi n)^{\frac{1}{r+1}}\lambda_l^{\frac{1}{2}} \sim c_r n^{\frac{1}{r+1}}l^{\frac{r}{r+1}}$, but with boundary values $\widetilde{\psi}_{l,n}(\pm 1)$ of magnitude

$$|\widetilde{\psi}_{l,n}(\pm 1)| \leq c_{r,\epsilon}\exp\left(-\left(\frac{\pi n}{r+1} - \epsilon\right)\right)$$

for any $\epsilon > 0$. By standard perturbation theory [32], near $\widetilde{\psi}_{l,n}(x), \widetilde{\omega}_{l,n}$ there exist *exact* eigenfunctions and eigenfrequencies $\psi_{l,n}(x)$, $\omega_{l,n}$ satisfying (2) and which are exponentially close (in n) to $\widetilde{\psi}_{l,n}(x), \widetilde{\omega}_{l,n}$; for the purpose of counting resonant frequencies of (1), we may thus work with the $\widetilde{\omega}_{l,n}$ to estimate $N(\omega)$. Ignoring constants, $n^{\frac{1}{r+1}}l^{\frac{r}{r+1}} \leq \omega$ if $n \leq \omega^{r+1}/l^r$, and the constraint $n \geq 1$ forces $l \leq \omega^{\frac{r+1}{r}}$, so one has

$$(3) \qquad N(\omega) \geq \sum_{l=1}^{\omega^{\frac{r+1}{r}}}\frac{\omega^{r+1}}{l^r} = \omega^{r+1}\sum_{l=1}^{\omega^{\frac{r+1}{r}}}\frac{1}{l^r},$$

which satisfies $N(\omega) \sim \omega^2 \cdot \log\omega$ if $r = 1$ and $N(\omega) \sim \omega^{r+1}$ if $r \geq 2$. For $r = 1$, compared with the classical Weyl power law (the growth rate of $N(\omega) \sim \omega^2$ for a 2D nondegenerate medium), the ideal SRO medium exhibits a *logarithmic* gain, while for $r \geq 2$, the rate is *polynomially* greater; in fact it is the same as Weyl's law for ∇^2 in dimension $r + 1$ (Figure 1).

In summary, the resonant frequency count for a 2D SRO medium has the same growth rate as for an $(r + 1)$-dimensional resonator. However, this is just one of the ways in which an SRO medium is superdimensional.

2.2. Anisotropic concentration of waves. SRO media also exhibit superdimensionality in the singularity strength of their Green's functions. For $\omega = 0$, the Green's function for (1) is known analytically [8, 9] and understood from a geometrical point of view for a more general class of equations [45]. In dimension 2, the Newtonian

potential $N(\mathbf{p})$ for a homogeneous, isotropic medium ($r = 0$), $N(\mathbf{p}) = \frac{1}{2\pi} \log |\mathbf{p}|$, is both rotation and translation invariant; fixing the pole at $\mathbf{p} = 0$, the singularity is logarithmic and the level curves are circles. In contrast, for $r \geq 1$, the Green's function $G(\mathbf{p}, \mathbf{q})$ for the SRO medium in (1) reflects both the inhomogeneity of the medium and the degeneracy along $x = 0$. Avoiding mathematical details and extracting from the literature only the structure needed here, the coefficient tensor of the operator in (1) is the inverse of a singular metric g in the rectangle R, with distance element

$$ds^2 = dx^2 + |x|^{-2r} dy^2.$$

This in turn corresponds to the optical length distance, $d(\mathbf{p}, \mathbf{q})$, for the wave propagation and defines a family of anisotropic "discs,"

$$B(\mathbf{p}, \delta) = \{\mathbf{q} \in \mathbb{R}^2 : d(\mathbf{q}, \mathbf{p}) < \delta\},$$

with center $\mathbf{p}$ and "radius" δ. The anisotropic discs are comparable to Euclidean discs away from $x = 0$, but flatten as one approaches the degeneracy axis $x = 0$, and those centered along the axis are comparable to $\delta \times \delta^{r+1}$ rectangles. Analysis shows that in the disc $B(\mathbf{0}, 1)$, of radius 1 centered at the origin, one can pack $\sim \delta^{-(r+1)}$ pairwise disjoint discs of radius δ. The Hausdorff fractal dimension [17] of R endowed with the optical length metric is $r + 1$, and the SRO material behaves as if it were a higher-dimensional space.

Consider the implications of this for the Green's function of (1). Denoting by $A(\mathbf{p}, \mathbf{q})$ the Euclidean area of the anisotropic disc $B(\mathbf{p}, d(\mathbf{p}, \mathbf{q}))$, the Green's function satisfies (see [44]) the estimate

$$(4) \qquad |G(\mathbf{p}, \mathbf{q})| \sim c \cdot \begin{cases} |\log A(\mathbf{p}, \mathbf{q})| + |\log A(\mathbf{q}, \mathbf{p})|, & r = 1, \\ \frac{d(\mathbf{p}, \mathbf{q})^2}{A(\mathbf{p}, \mathbf{q})} + \frac{d(\mathbf{q}, \mathbf{p})^2}{A(\mathbf{q}, \mathbf{p})}, & r \geq 2. \end{cases}$$

The explicit form of Green's functions, with a possibly nonzero frequency ω, has been computed, up to a smooth correction term, in the appendix. For $r \geq 2$, $\mathbf{p} = (0, p_2)$, and $\mathbf{q} = (q_1, q_2)$,

$$|G(\mathbf{p}, \mathbf{q})| \sim (|q_1| + |q_2 - p_2|^{\frac{1}{r+1}})^{-1};$$

see Figure 2(a). Waves for SRO media with point sources are thus both more singular than the logarithmic blow-up for standard media and, for $\mathbf{p}$ close to $x = 0$, anisotropically concentrated in highly eccentric sets (Figure 2(b)). Similar behavior of the Green's function holds for $\omega \neq 0$ (Figure 2(c, d)); this can be derived analytically from [8, 9], but we omit the somewhat involved derivations.

For the numerics, SRO resonators are modeled to occupy a rectangle R of width 2 and height 1 ($R = \{-1 \leq x \leq 1, -0.5 \leq y \leq 0.5\}$).[1] We are looking for the solution to the Helmholtz-type equation with a point source excitation and the Dirichlet BC $u = 0$ on the boundary. The equation considered is of the form

$$(5) \qquad \nabla \cdot \left(\overline{\overline{c}} \, \nabla u(\mathbf{x}) \right) + \omega^2 u(\mathbf{x}) = -\delta(\mathbf{x} - \mathbf{x}'),$$

where

$$(6) \qquad \overline{\overline{c}} = \begin{bmatrix} 1 & 0 \\ 0 & x^{2r} + a^{2r} \end{bmatrix},$$

---

[1] The simulations were performed using COMSOL Multiphysics version 4.4, based on the finite element method.

and $\mathbf{x}' = (x', y')$ is the location of the point source, and the minus sign is used for the graphics.

To ensure better numerical convergence and accuracy, especially when ω is increased, we only consider the case $r = 2$. Furthermore, the singularity in the ideal case cannot be properly captured by numerical methods. Hence we model an approximate SRO medium by setting the parameter $a = 0.1$ in (6).
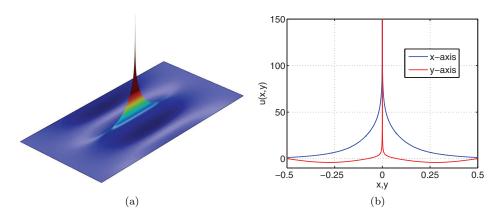

(a)   (b)

FIG. 4. *The Green's function $u(\mathbf{x})$ inside an approximate SRO resonator with $r = 2$, $a = 0.1$, $\omega = 2$, and $\mathbf{x}' = (0,0)$. (a) 3-dimensional (3D) surface plot. (b) Cross-cuts in x- and y-planes.*

Figure 4(a) presents a 3D surface plot of the Green's function $u(\mathbf{x})$ satisfying (5) with $\omega = 2$ and $\mathbf{x}' = (0,0)$. Figure 4(b) shows the cross-cuts of the solution in the x-plane ($y = 0$, $-0.5 \leq x \leq 0.5$) and the y-plane ($x = 0$, $-0.5 \leq y \leq 0.5$). The solution $u(\mathbf{x})$ is clearly seen to be strongly concentrated in the y-direction.

Figures 5(a), (b) shows similar plots for a higher frequency, $\omega = 5$. The profile of the solution in the x-plane is similar to the previous case, whereas almost all the oscillation is in the y-direction. Figure 5(c) further shows how the y-directed cross-sections of the solution change when moving away from the line $x = 0$.

2.3. Giant focusing of rays. Next consider the high frequency behavior of the Green's functions as $\omega \to \infty$. The rays through a given point can only point in directions that are combinations of $\frac{\partial}{\partial x}$ and $x^r \frac{\partial}{\partial y}$; passing through $x = 0$, motion is only allowed in the x-direction. This creates a giant focusing effect: all rays passing through a point $\mathbf{p}$ on the $x = 0$ axis focus horizontally at $\mathbf{p}$, having a common tangent vector at $\mathbf{p}$. Moreover, for any two points $\mathbf{p}$ and $\mathbf{q}$ that are on the axis $x = 0$, there are infinitely many rays connecting $\mathbf{p}$ and $\mathbf{q}$ [11, 12]. Reducing from the high frequency limit to a finite frequency ω, a wave produced by a point source at $\mathbf{p}$ still focuses strongly on many points on axis $x = 0$ (the focusing depends on the lengths of the connecting rays). At high ω, this produces strong concentration and large oscillation of the waves near $x = 0$ (Figure 2(c), (d)).

Following the analysis of [12], one can analytically solve and plot the rays for the corresponding 2D SRO medium. For an integer parameter $r \geq 1$, the standard 2D Grushin operator is

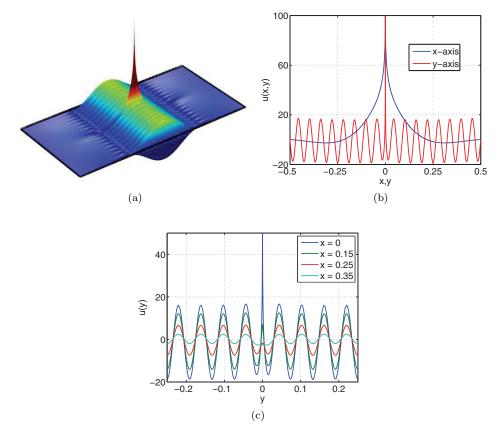$$L_r = \frac{1}{2} \left(\partial_x^2 + x^{2r} \partial_y^2 \right),$$

FIG. 5. *The Green's function $u(\mathbf{x})$ inside an approximate SRO resonator with $r = 2$, $a = 0.1$, $\omega = 5$, and $\mathbf{x}' = (0, 0)$. (a) 3D surface plot. (b) Cross-cuts in x- and y-planes. (c) Cross-sections in y-plane at different values of x.*

whose Hamiltonian is [12]

$$(7) \qquad H(x, y, \xi, \eta) = \frac{1}{2} \left(\xi^2 + x^{2r} \eta^2 \right).$$

Now restricting for simplicity to the case of $r = 2$, and considering the variables as functions of an independent variable t, the Hamiltonian system for the rays in phase space is

$$(8) \qquad \begin{cases} \frac{\mathrm{d}}{\mathrm{d}t} x(t) = \xi(t), \\ \frac{\mathrm{d}}{\mathrm{d}t} y(t) = \eta(t) x(t)^4, \\ \frac{\mathrm{d}}{\mathrm{d}t} \xi(t) = -2\eta(t)^2 x(t)^3, \\ \frac{\mathrm{d}}{\mathrm{d}t} \eta(t) = 0, \end{cases}$$

which can be solved numerically.[2] The rays are then the spatial coordinates $x(t)$ and $y(t)$ of the geodesics solving the system (8) with all possible initial conditions.

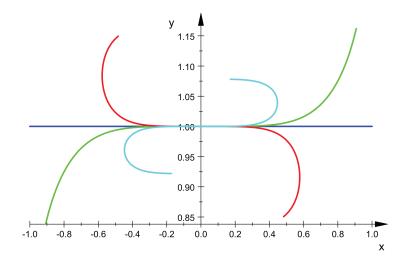[2]For instance, using MuPAD, which is an add-on for the Symbolic Math Toolbox in MATLAB.

FIG. 6. *SRO rays $(x(t), y(t))$ with $-1 \leq t \leq 1$ satisfying the ODE system* (8), *passing through the point* $\mathbf{x} = (0, 1)$. *The initial conditions are* $x(0) = 0$, $y(0) = 1$, *and* $\xi(0) = 1$ *and* $\eta(0) = 0$ *(blue),* $\eta(0) = 1$ *(green),* $\eta(0) = -3$ *(red), and* $\eta(0) = 5$ *(aqua).*
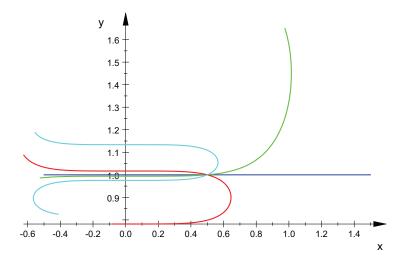

FIG. 7. *Rays $(x(t), y(t))$ with $-1 \leq t \leq 1$ satisfying the ODE system* (8), *passing through the point* $\mathbf{x} = (0.5, 1)$. *The initial conditions are* $x(0) = 0.5$, $y(0) = 1$, *and* $\xi(0) = 1$ *and* $\eta(0) = 0$ *(blue),* $\eta(0) = 1$ *(green),* $\eta(0) = -3$ *(red), and* $\eta(0) = 5$ *(aqua).*

Figure 6 shows segments of some of the rays passing through the point $\mathbf{x} = (x, y) = (0, 1)$, and Figure 7 shows rays passing through the point $\mathbf{x} = (0.5, 1)$. The curves are obtained plotting $y(t)$ with respect to $x(t)$ with parameter $-1 \leq t \leq 1$, with initial conditions $x(0) = 0$, $y(0) = 1$, and $\xi(0) = 1$. Different curves present rays with different values for $\eta(0)$. The behavior of the rays illustrates the strong focusing effect in the Grushin material. As seen in Figure 6, when approaching a point on the $x = 0$ line, the light rays incident from different directions concentrate on the same path and have a common (horizontal) tangent at the point $(0, y)$.

3. Approximate SRO. The ideal SRO medium of (1), having the infinitely large anisotropy at $x = 0$, is not physically realizable. In order to specify, in section 6 below, SRO designs which are realistic for physical implementation, we first describe approximations to the ideal SRO parameters of section 2. For a dimensionless parameter $0 < a < 1$, an approximate SRO medium is modeled by the elliptic PDE

$$(9) \qquad (\partial_x^2 + (a^{2r} + x^{2r})\partial_y^2)u(\mathbf{p}) + \omega^2 u(\mathbf{p}) = 0, \quad \mathbf{p} \in R.$$

The maximum degeneracy occurs at $x = 0$, and the anisotropy does not vary greatly in the strip $|x| \leq a$; outside of this strip, the approximate SRO medium is close to the ideal medium (1). Consider the eigenvalues and eigenfunctions of (9) with the Dirichlet BC, $u = 0$. Modifying the analysis above, the spectrum for (2) is shifted by $\pi^2 n^2 a^{2r}$, so that (9) has eigenfrequencies $\omega_{l,n}(a)$ exponentially close to

$$\widetilde{\omega}_{l,n}(a) := (\widetilde{\omega}_{l,n}^2 + \pi^2 n^2 a^{2r})^{\frac{1}{2}} \sim (c_r^2 n^{\frac{2}{r+1}} l^{\frac{2r}{r+1}} + \pi^2 a^{2r} n^2)^{\frac{1}{2}} \sim c_r n^{\frac{1}{r+1}} l^{\frac{r}{r+1}} + \pi a^r n.$$

The condition $\widetilde{\omega}_{l,n}(a) \leq \omega$ constrains both $a^{2r} n^2 \lesssim \omega^2$, so that $n \lesssim a^{-r}\omega$, and $n^{\frac{1}{r+1}} l^{\frac{r}{r+1}} \leq \omega^2$, so that $n \lesssim \omega^{r+1}/l^r$. (Here, we are using $\lesssim$ to suppress inessential dependence on constants such as π and c_r.) Hence, temporarily fixing ω, $\widetilde{\omega}_{l,n} \leq \omega$ implies that $n \lesssim \min(\frac{\omega}{a^r}, \frac{\omega^{r+1}}{l^r})$, and the transition between the two takes place when $\omega = l/a$. In the low frequency regime, $\omega \lesssim \Omega(a) := a^{-1}$, one has $a\omega < 1$ and the counting function $N(\omega, a) := \#\{\omega_{l,n}(a) : \omega_{l,n}(a) \leq \omega\}$ satisfies

$$N(\omega, a) \sim n^{1/(r+1)} \ell^{r/(r+1)} \leq \omega,$$

which yields the same superdimensional size estimate as in (3) for the ideal SRO medium. On the other hand, for $\omega \geq \Omega(a)$, decompose the sum in l into

$$\sum_{l=1}^{a\omega} \frac{\omega}{a^r} + \sum_{l=a\omega}^{\omega^{\frac{r+1}{r}}} \frac{\omega^{r+1}}{l^r},$$

leading to a quadratic lower bound of

$$N(\omega, a) \geq a^{1-r}\omega^2 + a^{1-r}\omega^2.$$

Let $\Omega_{r,a} = \sqrt{c_r}a^{-1}$. For $r \geq 2$ and $\delta > 0$, the number of $\omega_{l,n}$ in the band $(1-\delta)\Omega(a) \leq \omega \leq (1+\delta)\Omega_{r,a}$ is $\sim \delta\Omega_{r,a}^{r+1}$, retaining the superdimensionality of the ideal SRO medium, while in the high frequency limit $\omega \to \infty$, the growth rate of $N(\omega, a)$ is quadratic, as is dictated by Weyl's law in dimension 2.

4. Effective medium theory for SRO metamaterials. The scalar Helmholtz equation considered here, of the form

$$(10) \qquad \left((\partial_x^2 + (a^{2r} + x^{2r})\partial_y^2) + \omega^2\right) u(\mathbf{x}) = 0,$$

holds, for example, for the z-component of the magnetic field of a transverse electric (TE), or more precisely, TE_z-polarized electromagnetic wave propagating in the approximate SRO medium for approximation parameter a in the xy-plane. Here, the permittivity $\overline{\overline{\varepsilon}}$ in the xy-plane is inhomogeneous and anisotropic,

$$(11) \qquad \overline{\overline{\varepsilon}} = \varepsilon_0 \begin{bmatrix} \varepsilon_{xx} & 0 & 0 \\ 0 & \varepsilon_{yy} & 0 \\ 0 & 0 & \varepsilon_{zz} \end{bmatrix},$$

with

$$\varepsilon_{xx} = \frac{1}{a^{2r} + x^{2r}} \text{ and } \varepsilon_{yy} = 1. \tag{12}$$

The permittivity component ε_{zz}, perpendicular to the plane, is irrelevant, as the electric field has no z-component. Also the material is assumed to be nonmagnetic, with permeability $\overline{\overline{\mu}} = \mu_0 \overline{\overline{I}}$, with μ_0 constant.

For the effective medium theory of the approximate SRO medium, we introduce length scales d, D such that

$$d \ll aD \leq D, \tag{13}$$

where the resonator will be of size $D \times D$ and the MM cells will be of size $d \times d$. Thus, we consider the resonator $\{(x, y) \in \mathbb{R}^2 : |x| < \frac{D}{2}, |y| < \frac{D}{2}\}$ with relative permittivity given by

$$\varepsilon_{xx} = \frac{1}{a^{2r} + (\frac{x}{D})^{2r}} \text{ and } \varepsilon_{yy} = 1. \tag{14}$$

For time-harmonic waves with a $e^{i\omega t}$ time dependence (where $i = \sqrt{-1}$), Maxwell's equations become

$$\nabla \times \mathbf{E} = i\omega \mathbf{B} = i\omega \mu_0 \mathbf{H}, \tag{15}$$

$$\nabla \times \mathbf{H} = -i\omega \mathbf{D} = -i\omega \overline{\overline{\varepsilon}} \cdot \mathbf{E}. \tag{16}$$

Note that $\omega = 2\pi c_0/\lambda_0$, with λ_0 the free-space wavelength, and we now assume that D is of the same order of magnitude as λ_0.

Since the TE_z wave consists of the fields

$$\mathbf{E} = \mathbf{u}_x E_x + \mathbf{u}_y E_y, \tag{17}$$

$$\mathbf{H} = \mathbf{u}_z H_z, \tag{18}$$

here and below, $\mathbf{u}_x$, $\mathbf{u}_y$, and $\mathbf{u}_z$ denote the unit coordinate vectors $(1, 0, 0)$, $(0, 1, 0)$, and $(0, 0, 1)$, respectively. Faraday's law (15) gives

$$\mathbf{u}_z \left(\frac{\partial}{\partial x} E_y - \frac{\partial}{\partial y} E_x \right) = -\mathbf{u}_z i\omega \mu_0 H_z. \tag{19}$$

Then, from Ampère's law (16), we get

$$\mathbf{u}_x \frac{\partial}{\partial y} H_z - \mathbf{u}_y \frac{\partial}{\partial x} H_z = -i\omega\varepsilon_0 (\mathbf{u}_x \varepsilon_{xx} E_x + \mathbf{u}_y \varepsilon_{yy} E_y), \tag{20}$$

from which we can solve

$$E_x = \frac{i}{\omega\varepsilon_0\varepsilon_{xx}} \frac{\partial}{\partial y} H_z, \tag{21}$$

$$E_y = -\frac{i}{\omega\varepsilon_0\varepsilon_{yy}} \frac{\partial}{\partial x} H_z. \tag{22}$$

Substituting the obtained E_x and E_y into (19) gives us the following equation for H_z:

$$\frac{1}{\varepsilon_{yy}} \frac{\partial^2}{\partial x^2} H_z + \frac{1}{\varepsilon_{xx}} \frac{\partial^2}{\partial y^2} H_z + \omega^2 \varepsilon_0 \mu_0 H_z = 0. \tag{23}$$

Let $k = \omega\sqrt{\epsilon_0\mu_0}$ be the wave number; then in physical units, (23) becomes

$$(24) \qquad \left(\frac{\partial^2}{\partial x^2} + \left(a^{2r} + \left(\frac{x}{D}\right)^{2r} \right) \frac{\partial^2}{\partial y^2} + k^2 \right) H_z = 0.$$

Now consider the approximate material as in (14). A simple possible approach towards an effective material having this kind of anisotropic effective permittivity is to construct the SRO medium as a lattice of subwavelength scale unit cells, where each $d \times d$ sized cell consists of a strip parallel to the x-axis, of variable width $w(x)$, and of extremely high relative permittivity ε_h (dimensionless), embedded in background material with relative permittivity $\varepsilon_r = 1$ (Figure 8). We choose the width $w(x)$, and hence the fill ratios, $w(x)/d$, so that the first equation in (14) is satisfied in the homogenization limit, and then we show that the second is approximately satisfied.
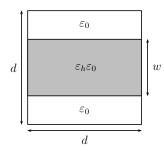

FIG. 8. *The structure of one MM cell in the lattice that forms the effectively homogeneous 2D SRO material. Each cell consists of a horizontal strip of material with a high permittivity $\varepsilon_h\varepsilon_0$, embedded in the background material with permittivity ε_0. These cells are assembled horizontally with varying fill ratios $w(x)/d$, and the resulting strips then stacked vertically.*

Based on series and parallel connections of capacitances, the effective permittivities ε_{xx} and ε_{yy} of a single unit cell can be written analytically as

$$(25) \qquad \varepsilon_{xx}(x) = (\varepsilon_h - 1)\frac{w(x)}{d} + 1, \quad \varepsilon_{yy}(x) = \frac{\varepsilon_h}{(1 - \varepsilon_h)\frac{w(x)}{d} + \varepsilon_h}.$$

Note that we do not have enough free parameters to make the permittivities in (25) match exactly those in (14), and a further approximation must be introduced. Fortunately the strip width $w(x)$ has a much larger effect on ε_{xx} than on ε_{yy}. Therefore, as the distance x varies, we can set the strip width $w(x)$ to have the profile

$$(26) \qquad w(x) = \frac{1}{\varepsilon_h - 1} \left(\frac{1}{(x/D)^{2r} + a^{2r}} - 1 \right) d, \quad \text{for } |x| < \frac{D}{2},$$

which gives us the specifications for a realistic SRO medium:

$$(27) \qquad \varepsilon_{xx} = \frac{1}{(x/D)^{2r} + a^{2r}}, \quad \varepsilon_{yy} = \frac{\varepsilon_h((x/D)^{2r} + a^{2r})}{(\varepsilon_h + 1)((x/D)^{2r} + a^{2r}) - 1}.$$

This ε_{xx} exactly satisfies (14), and also provides a reasonable approximation to the second equation in (14), as long as $\epsilon_h \gg (1/a)^{2r}$. Conversely, for strip material with high relative permittivity ϵ_h, we can implement the approximate SRO parameters (14) for $a \gg 1/\epsilon_h^{1/2r}$.

5. Parameter constraints. To summarize the discussion so far: In order to specify an effective SRO medium achieving the superdimensional characteristics of an SRO medium of order r, fix

(i) a frequency ω_0 defining the band in which one wants to work;

(ii) a length size D of the desired resonator; and

(iii) the relative permittivity $\epsilon_h \gg 1$ of the material to be used in constructing the MM cells.

Then, if

$$\text{(28)} \qquad \epsilon_h \gg \left(D\omega_0\sqrt{\epsilon_0\mu_0}\right)^{2r},$$

there is an interval for the parameters a, given by the inequalities

$$\text{(29)} \qquad \epsilon_h^{-1} \ll a^{2r} \lesssim \min\left(1, (D\omega_0\sqrt{\epsilon_0\mu_0})^{-2r}\right),$$

for which it is possible to construct a resonator effectively implementing the approximate SRO medium of order r and approximation parameter a near the frequency ω_0. We now turn to a particular implementation.

6. Implementation. With the goal of constructing a microwave SRO resonator structure as in (27) for $r = 2$, the next issue is to find a dielectric material with ε_h as large as possible. [31] reported that a barium titanate (BaTiO$_3$) ceramic can be prepared so as to exhibit a permittivity with real part as high as $\varepsilon_h \approx 2700$ at $f = 1$GHz. From [31, Figure 6], it can be seen that the imaginary part has a local minimum close to this frequency. Assuming that one has a material with permittivity $\varepsilon_h = 2700$ and neglecting the effects of losses and frequency dispersion, we get an idealized insight of how a superdimensional resonator could be constructed. The size of the resonator is defined by the scaling parameter D, so that the constraint $-D < x < D$ implies that $-1 < x/D < 1$. As the free-space wavelength at $f = 1$GHz is $\lambda_0 = 0.3m$, choose $D = 0.2m$. Then $(D\omega_0\sqrt{\epsilon_0\mu_0})^{-1} \approx 0.24$ and, for $a = 0.23$, $r = 2$, we have $a^4\varepsilon_h \approx 7.6$; i.e., (28) and (29) are satisfied. Moreover, the maximum value for ε_{xx} in (27) at $x = 0$ becomes $\varepsilon_{xx} \approx 357$. In contrast, ε_{yy} remains very close to unity, with its maximum value at $x = 0$ being $\varepsilon_{yy} \approx 1.15$. As for w, it becomes 0 at $x \approx 0.997D$.

In Figure 9(a) we present the width profile w/D of the strip as a function of x while Figure 9(b) shows a schematic of the realization of the resonator. In these figures we take $a = 0.15$, so that $a^4\varepsilon_h$ is just 1.4; the behavior of ε_{xx} and ε_{yy} as functions of x for this a is presented in Figure 10. Note that now $\varepsilon_{xx}(0) \approx 1961$; however, ε_{yy} ranges from 1 to 3.7. Nevertheless, simulations performed using CM show that the superdimensional wave concentration still holds; see Figure 11. In summary, the qualitative features of the superdimensionality discussed above persist for an approximation parameter as large as $a = 0.15$, demonstrating the robustness of the SRO phenomena.

Also observe that, since the waves can travel much faster in the x-direction, the resonator is most efficiently excited by a $\mathbf{u}_y$-oriented (line) dipole. Figures 11(a) and 11(b) show the absolute value of the magnetic field $|H_z|$ in the resonator, which is excited using a line dipole with $f = 1$GHz at different locations. Again, despite the approximations made in the material parameters, the strong wave concentration effect is observed. The implemented resonator works qualitatively, demonstrating that the SRO phenomenon is robust.
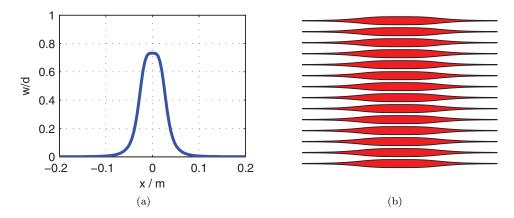
FIG. 9. (a) *The ratio between the width of the strip w and the side length of the unit cell d as a function of x throughout the resonator.* (b) *Schematic drawing of the resonator near $x = 0$.*
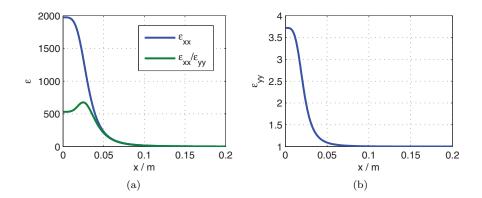

FIG. 10. (a) *The effective homogenized ε_{xx} compared with the ratio between ε_{xx} and ε_{yy}.* (b) *Effective ε_{yy}. The maximum of the anisotropy ratio $\varepsilon_{xx}/\varepsilon_{yy}$ has shifted from $x = 0$ to $|x| \approx 0.025m$. As both permittivity components are symmetric with respect to x, they are plotted only with $0 < x < D$.*

7. Variations.

7.1. Bulk SRO. Similar ideas allow for the SRO paradigm to be applied in dimension 3. An ideal bulk SRO material in $Q = \{\mathbf{p} = (x, y, z) : |x| \leq 1, 0 \leq y \leq 1, 0 \leq z \leq 1\}$ may be modeled by replacing (1) with $u = 0$ on ∂Q and

$$(30) \qquad \left(\partial_x^2 + x^{2r}\left(\partial_y^2 + \partial_z^2\right) + \omega^2\right)u(\mathbf{p}) = 0 \text{ on } Q.$$

For $\mathbf{n} = (n_1, n_2) \in \mathbb{Z}_+^2$, eigenfunctions of the form $u(\mathbf{p}) = \psi_{\mathbf{n}}(x)\sin(\pi n_1 y)\sin(\pi n_2 z)$, where $\psi_{\mathbf{n}}$ must satisfy (2) with n^2 replaced by $\mathbf{n}^2 := n_1^2 + n_2^2$. As above, one constructs approximate spectral data $\widetilde{\psi}_{l,\mathbf{n}}, \widetilde{\omega}_{l,\mathbf{n}}$, admitting exact solution perturbations $\psi_{l,\mathbf{n}}, \omega_{l,\mathbf{n}}$, exponentially nearby (in $|\mathbf{n}|$), and to estimate $N(\omega)$, it suffices to work with $\widetilde{\omega}_{l,\mathbf{n}}$. As in the 2D case, we need both $|\mathbf{n}|^{\frac{1}{r+1}}l^{\frac{r}{r+1}} \leq \omega$, which holds off $|\mathbf{n}| \leq \omega^{r+1}/l^r$,
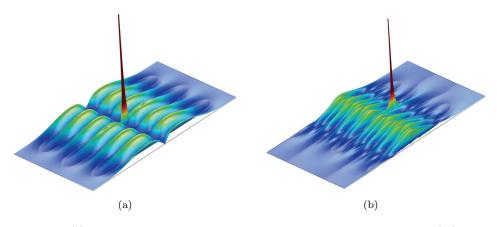
FIG. 11. (a) *Superdimensional electromagnetic resonator with material parameters* (27) *excited by a* $\mathbf{u}_y$*-polarized line dipole at* $(x', y') = (0, 0)$ *at* $f = 1\,GHz$. (b) *Same as in* (a) *but with the dipole located at* $(x', y') = (0.05m, 0m)$.

and $|\mathbf{n}| \geq 1$, so that $l \leq \omega^{\frac{r+1}{r}}$. Since $\mathbf{n}$ is 2D,

$$N(\omega) \geq \sum_{l=1}^{\omega^{(r+1)/r}} \frac{\omega^{2(r+1)}}{l^{2r}} = c_r \omega^{2r+2},$$

so that this 3D ideal SRO design exhibits a $(2r+2)$-dimensional eigenfrequency count. For the least degenerate case, $r = 1$, this is already 4-dimensional.

As with the 2D case, a more realistic 3D SRO design is an approximate one at length scale a, with the x^{2r} in (30) replaced by $a^{2r} + x^{2r}$, and this exhibits the superdimensionality in frequency bands about $\Omega = (c_r)^{1/r} a^{-1}$. The 3D approximate SRO medium produces, as in the 2D case, a frequency shift from the ideal, $\omega \to (\omega^2 + a^{2r})^{\frac{1}{2}}$. When a is small enough, the Green's function is close to the ideal Green's function that has a strong singularity when the source point is at the surface $x = 0$. For high frequencies it exhibits the ideal medium's strong concentration of rays and waves.

7.2. General SRO designs. The examples presented here are chosen to have symmetries permitting analysis using quantum oscillators in 1D. However, the same principles, and resulting superdimensionality, apply to general SRO designs. A standard Riemannian metric $g(\mathbf{p}) = (g_{jk})$ in dimension 3 satisfies

$$c_1 |\mathbf{v}|^2 \leq \sum_{j,k=1}^{3} g_{jk}(\mathbf{p}) v^j v^k \leq c_2 |\mathbf{v}|^2,$$

where $\mathbf{v} = (v^1, v^2, v^3)$, for some $0 < c_1 \leq c_2 < \infty$. The dual metric, $g^{-1} = (g^{jk})$, satisfies

$$(c_2)^{-1} |\xi|^2 \leq \sum_{j,k=1}^{3} g^{jk}(\mathbf{p}) \xi_j \xi_k \leq (c_1)^{-1} |\xi|^2$$

for all $\xi = (\xi_1, \xi_2, \xi_3)$. For a *sub-Riemannian* metric, (i) $c_2 = +\infty$ is allowed, so that g is singular and $(c_2)^{-1} = 0$, so that g^{-1} is degenerate, with the velocity in the corresponding directions equal to 0, and (ii) a global condition is imposed that

any two points can be connected to each other by a geodesic (i.e., a ray) of g. In SRO media, corresponding to an SR metric, the waves are modeled by the Helmholtz equation,

$$\sum_{j,k=1}^{3} \partial_j(g^{jk}(\mathbf{p})\partial_k u(\mathbf{p})) + \omega^2 u(\mathbf{p}) = 0.$$

The variety of SR geometries available [43] allows for many asymmetric variations of the SRO designs described here; the extensive mathematical literature, e.g., [41, 18, 45, 44], shows that the superdimensionality of the eigenfrequency count and the concentration of waves will hold for these more general SRO media.

8. Discussion and conclusions. We have described MM arrays exhibiting superdimensional behaviors such as giant focusing and high density of resonant frequencies. Possible applications of SRO include components for antennas that have a high density of resonance frequencies in a desired frequency band, materials in which point sources produce fields having anomalously strong blow-up, and optical materials with giant focusing that either guide light rays together or separate closely propagating rays.

Appendix: Anisotropic singularity of Green's function. In this appendix we provide the details of the analysis of Green's functions in an ideal SRO material; see Figures 2 and 4. Let $L = L(\mathbf{x}, D_\mathbf{x})$ be the partial differential operator on the square $\Omega = [-1, 1]^2$ in dimension 2,

$$L(\mathbf{x}, D_\mathbf{x})u(\mathbf{x}) = (\partial_x^2 + x^4 \partial_y^2)u(\mathbf{x}),$$

where we use coordinates $\mathbf{x} = (x, y) \in \mathbb{R}^2$. $L(\mathbf{x}, D_\mathbf{x})$ is a special case, for $r = 2$, of the operator family

$$L_r(\mathbf{x}, D_\mathbf{x})u(\mathbf{x}) = (\partial_x^2 + x^{2r} \partial_y^2)u(\mathbf{x}).$$

These degenerate elliptic partial differential operators are the so-called Grushin operators [29]. We compute the Green's function, $G_\omega(\mathbf{x}; \mathbf{x}') = G_\omega(x, y; x', y')$, $\omega \in \mathbb{R}$, such that

$$(31) \qquad (L(\mathbf{x}, D_\mathbf{x}) + \omega^2)G_\omega(\mathbf{x}; \mathbf{x}') = \delta(\mathbf{x} - \mathbf{x}'), \quad \mathbf{x}, \mathbf{x}' \in \Omega = [-1, 1]^2,$$
$$(32) \qquad G_\omega(\mathbf{x}; \mathbf{x}')|_{\mathbf{x} \in \partial\Omega} = 0.$$

For $\omega > 0$, G_ω is uniquely defined as long as ω^2 is not a Dirichlet eigenvalue of $L + \omega^2$ in Ω.

Next we construct an approximation to G_ω^{app} by using an auxiliary 3D problem. Let $g(\mathbf{r}; \mathbf{r}')$, $\mathbf{r} = (x, y, x)$, $\mathbf{r}' = (x', y', x') \in \mathbb{R}^3$ be the free-space Green's function of the 3D equation

$$(33) \qquad (\partial_x^2 + x^4 \partial_y^2 + \partial_z^2)g(x, y, z; x', y', z') = \delta(x - x')\delta(y - y')\delta(z - z').$$

We define an approximation to $G_\omega^{\mathrm{app}}(\mathbf{x}; \mathbf{x}') \approx G_\omega(\mathbf{x}; \mathbf{x}')$ by setting

$$(34) \qquad G_\omega^{\mathrm{app}}(x, y; x', y') = \int_\mathbb{R} g(x, y, z; x', y', 0)\phi(z)\mathrm{d}z,$$

and $\phi(z) \in C_0^\infty(\mathbb{R})$ is a function that vanishes outside interval $(-3, 3)$ and satisfies $\int_\mathbb{R} \phi(z)dz = 1$, $\phi(0) = 1$. To obtain convenient formulas below, use a function ϕ such that $\phi(z) = e^{\omega z}$ when $z \in (-1, 1)$.

Because $g(\mathbf{r}, \mathbf{r}')$ satisfies (33) and $\phi(0) = 1$, it follows that

$$(L + \omega^2)G_\omega^{\mathrm{app}} = \delta(x - x')\delta(y - y') + F(x, y; x', y'),$$

where

$$F(x, y, x', y') = \int_{\mathbb{R}} g(x, y, z; x', y', 0)a(z)\mathrm{d}z$$

and $a(z) = (\omega^2 - \partial_z^2)\phi(z)$. One can then write $G_\omega = G_\omega^{\mathrm{app}} + G_\omega^{\mathrm{corr}}$, where the correction term G_ω^{corr} satisfies the boundary value problem,

$$(L + \omega^2)G_\omega^{\mathrm{corr}}(x, y; x', y') = -F(x, y; x', y'), \quad (x, y) \in \Omega,$$
$$G_\omega^{\mathrm{corr}}(\mathbf{x}, \mathbf{x}') = -G_\omega^{\mathrm{app}}(\mathbf{x}, \mathbf{x}') \text{ for } \mathbf{x} \in \partial\Omega.$$

Since $a(z) = (\omega^2 - \partial_z^2)e^{\omega z} = 0$ when $z \in [-1, 1]$, we see that $F(x, y; x', y')$ is C^∞-smooth in the whole space $\mathbb{R}^2 \times \mathbb{R}^2$. Since $L(\mathbf{x}, D)$ is a hypoelliptic operator [30] and F is C^∞-smooth and the above implies that $\mathbf{x} \mapsto G_\omega^{\mathrm{corr}}(\mathbf{x}, \mathbf{x}')$ is a C^∞-smooth function in Ω, then $\mathbf{x} \mapsto G_\omega(\mathbf{x}, \mathbf{x}') - G_\omega^{\mathrm{app}}(\mathbf{x}, \mathbf{x}')$ is a C^∞-smooth function.

In summary, the functions $G_\omega(\mathbf{x}; \mathbf{x}')$ and $G_\omega^{\mathrm{app}}(\mathbf{x}; \mathbf{x}')$ are smooth outside the diagonal $\{\mathbf{x} = \mathbf{x}'\}$ and have the same asymptotics near $\{\mathbf{x} = \mathbf{x}'\}$ to all orders. The function G_ω^{app} is defined by formula (34), using the Green's function $g(\mathbf{x}; \mathbf{x}')$ of (33) in $\mathbb{R}^3$. This function $g(\mathbf{x}, \mathbf{x}')$ has an analytical representation given by Beals, Greiner, and Gaveau [9], who studied the general family of degenerate elliptic operators on $\mathbb{R}^{n+m}$,

$$(35) \qquad L(\mathbf{u}, \mathbf{t}, D) = L_{nmk} = \sum_{j=1}^{n} \frac{\partial^2}{\partial\mathbf{u}_j^2} + |\mathbf{u}|^{2k-2} \sum_{j=1}^{m} \frac{\partial^2}{\partial t_j^2}.$$

The operator in (33) is a special case of (35) with indices $n = 2$, $m = 1$, and $k = 3$, where we group the variables as $\mathbf{u} = (x, z) \in \mathbb{R}^2$, $\mathbf{t} = y \in \mathbb{R}$, and $\mathbf{r} = (\mathbf{u}, \mathbf{t}) \in \mathbb{R}^3$:

$$L_{213}(\mathbf{r}, D) = P(\mathbf{u}, \mathbf{t}, D) = (\partial_x^2 + \partial_z^2 + x^4\partial_y^2).$$

A free-space Green's function K_{nmk} for $L_{nmk}(\mathbf{r}, D)$, derived in [9, Theorem 2], satisfying

$$L_{nmk}(\mathbf{r}, D)[K_{nmk}(\mathbf{r}; \mathbf{r}')] = \delta(\mathbf{r} - \mathbf{r}'),$$

has an exact form,

$$(36) \qquad K_{nmk} = c_{nmk}\frac{F_{nmk}}{R^{\frac{n+mk-2}{2k}}},$$

where c_{nmk} is a constant and F_{nmk} and R are functions of $\mathbf{r} = (x, y, z)$ and $\mathbf{r}' = (x', y', z')$. Generally following the notation of [9], we define

$$R = R(\mathbf{r}, \mathbf{r}') = \frac{1}{2}\left(x^6 + z^6 + (x')^6 + (z')^6 + 9(y - y')^2\right)$$

and

$$\rho = \rho(\mathbf{x}; \mathbf{x}') = \frac{(x^2 + z^2)^{3/2}((x')^2 + (z')^2)^{3/2}}{R(x, y, z, x', y', z')}$$

and

$$v = v(\mathbf{x}; \mathbf{x}') = \frac{xx' + zz'}{(x^2 + z^2)^{1/2}((x')^2 + (z')^2)^{1/2}}.$$

In terms of $R = R(\mathbf{x}; \mathbf{x}')$, $\rho = \rho(\mathbf{x}; \mathbf{x}')$, and $v = v(\mathbf{x}; \mathbf{x}')$, the function $g(\mathbf{x}; \mathbf{x}')$ is given by

(37) $$g(\mathbf{r}; \mathbf{r}') = K_{213}(\mathbf{r}; \mathbf{r}') = -\frac{3}{8\pi^{3/2}} \frac{F_{213}(v, \rho))}{R(\mathbf{r}; \mathbf{r}')^{\frac{1}{2}}},$$

where

$$F_{213}(v, \rho) = \frac{1}{\Gamma(1/4)^2} \int_0^1 \int_0^1 \frac{F_{223}(v, u_1^{1/2} u_2^{1/2} \rho)}{u_1^{3/4} u_2^{1/4} (1 - u_1)^{3/4} (1 - u_2)^{3/4}} \, du_1 du_2$$

and

$$F_{223}(v, s) = \frac{\phi_-(s^2)}{(\phi_+(s^2) - 2s^{\frac{1}{3}} v) \sqrt{1 - s^2}},$$

where

$$\phi_\pm(s^2) = (1 + \sqrt{1 - s^2})^{\frac{1}{3}} \pm (1 - \sqrt{1 - s^2})^{\frac{1}{3}}.$$

In summary, Green's function $G_\omega(\mathbf{x}, \mathbf{x}')$ is a sum of a function $G_\omega^{\mathrm{corr}}(\mathbf{x}, \mathbf{x}')$ that is C^∞-smooth in the $\mathbf{x}$ variable and the function

$$\begin{aligned} G_\omega^{\mathrm{app}}(x, y; x', y') &= \int_{\mathbb{R}} g(x, y, z; x', y', 0)\phi(z)\mathrm{d}z \\ &= -\int_{\mathbb{R}} \frac{3}{8\pi^{3/2}} \frac{F_{123}(x, y, z; x', y', 0)}{R(x, y, z; x', y', 0)^{1/2}} \phi(z)\mathrm{d}z, \end{aligned}$$

and $\phi(z)$ is a C^∞-smooth function that vanishes outside a bounded interval and satisfies $\int_{\mathbb{R}} \phi(z)dz = 1$, $\phi(0) = 1$, and moreover, $\phi(z) = e^{\omega z}$ when $z \in (-1, 1)$. This explicit representation shows how anisotropic the singularity of Green's function $G_\omega(\mathbf{x}, \mathbf{x}')$ is near the critical line $x = 0$.

REFERENCES

[1] H. AMMARI, P. MILLIEN, M. RUIZ, AND H. ZHANG, *Mathematical analysis of plasmonic nanoparticles: The scalar case*, Arch. Ration. Mech. Anal., 224 (2017), pp. 597–658.

[2] H. AMMARI AND H. ZHANG, *Super-resolution in high-contrast media*, Proc. A., 471 (2015), 20140946.

[3] H. AMMARI AND H. ZHANG, *A mathematical theory of super-resolution by using a system of sub-wavelength Helmholtz resonators*, Comm. Math. Phys., 337 (2015), pp. 379–428.

[4] H. AMMARI, B. FITZPATRICK, H. LEE, S. YU, AND H. ZHANG, *Subwavelength phononic bandgap opening in bubbly media*, J. Differential Equations, 263 (2017), pp. 5610–5629.

[5] H. AMMARI, H. KANG, H. LEE, M. LIM, AND S. YU, *Enhancement of near cloaking for the full Maxwell equations*, SIAM J. Appl. Math., 73 (2013), pp. 2055–2076.

[6] G. BAO AND H. LIU, *Nearly cloaking the electromagnetic fields*, SIAM J. Appl. Math., 74 (2014), pp. 724–742.

[7] G. BAO AND H. LIU, *Nearly cloaking the full Maxwell equations: Cloaking active contents with general conducting layers*, J. Math. Pures Appl., 101 (2014), pp. 716–733.

[8] R. BEALS, *A note on fundamental solutions*, Comm. Partial Differential Equations, 24 (1999), pp. 369–376.

[9] R. BEALS, P. GREINER, AND B. GAVEAU, *Green's functions for some highly degenerate elliptic operators*, J. Funct. Anal., 165 (1999), pp. 407–429.

[10] R. BEALS, P. GREINER, AND B. GAVEAU, *Erratum to "Green's functions for some highly degenerate elliptic operators,"* J. Funct. Anal., 201 (2003), p. 301.

[11] O. CALIN, D.-C. CHANG, P. GREINER, AND Y. KANNAI, *On the geometry induced by a Grushin operator*, in Complex Analysis and Dynamical Systems II, Contemp. Math. 382, AMS, Providence, RI, 2005, pp. 89–111.

[12] D.-C. Chang and Y. Li, *SubRiemannian geodesics in the Grushin plane*, J. Geom. Anal., 22 (2012), pp. 800–826.

[13] H.-Y. Chen and C. T. Chan, *Transformation media that rotate electromagnetic fields*, Appl. Phys. Lett., 90 (2007), 241105.

[14] H.-Y. Chen, J. Yang, J. Zi, and C. T. Chan, *Transformation media for linear liquid surface waves*, Europhys. Lett., 85 (2009), 24004.

[15] S. Cummer et al., *Scattering theory derivation of a 3D acoustic cloaking shell*, Phys. Rev. Lett., 100 (2008), 024301.

[16] Y. Deng, H. Liu, and G. Uhlmann, *Full and partial cloaking in electromagnetic scattering*, Arch. Ration. Mech. Anal., 223 (2017), pp. 265–299.

[17] K. J. Falconer, *The Geometry of Fractal Sets*, Cambridge Tracts in Math. 85, Cambridge University Press, 1986.

[18] C. Fefferman and D. H. Phong, *On the asymptotic eigenvalue distribution of a pseudo differential operator*, Proc. Nat. Acad. Sci. U.S.A., 77 (1980), pp. 5622–5625.

[19] A. Greenleaf, Y. Kurylev, M. Lassas, and G. Uhlmann, *Electromagnetic wormholes and virtual magnetic monopoles from metamaterials*, Phys. Rev. Lett., 99 (2007), 183901.

[20] A. Greenleaf, Y. Kurylev, M. Lassas, and G. Uhlmann, *Approximate quantum cloaking and almost-trapped states*, Phys. Rev. Lett., 101 (2008), 220404.

[21] A. Greenleaf, Y. Kurylev, M. Lassas, and G. Uhlmann, *Invisibility and inverse problems*, Bull. Amer. Math. Soc. (N.S.), 46 (2009), pp. 55–97.

[22] A. Greenleaf, Y. Kurylev, M. Lassas, and G. Uhlmann, *Electromagnetic wormholes via handlebody constructions*, Comm. Math. Phys., 281 (2008), pp. 369–385.

[23] A. Greenleaf, Y. Kurylev, M. Lassas, and G. Uhlmann, *Approximate quantum and acoustic cloaking*, J. Spectral Theory, 1 (2011), pp. 27–80.

[24] A. Greenleaf, Y. Kurylev, M. Lassas, and G. Uhlmann, *Cloaking a sensor via transformation optics*, Phys. Rev. E, 83 (2011), 016603.

[25] A. Greenleaf, Y. Kurylev, M. Lassas, and G. Uhlmann, *Cloaking devices, electromagnetic wormholes, and singular transformation optics*, SIAM Rev., 51 (2009), pp. 3–33.

[26] A. Greenleaf, Y. Kurylev, M. Lassas, U. Leonhardt, and G. Uhlmann, *Schrodinger's Hat: Electromagnetic, acoustic and quantum amplifiers via transformation optics*, Proc. Natl. Acad. Sci. USA, 109 (2012), pp. 10169–10174.

[27] A. Greenleaf, M. Lassas, and G. Uhlmann, *On nonuniqueness for Calderon's inverse problem*, Math. Res. Lett., 10 (2003), pp. 685–693.

[28] A. Greenleaf, M. Lassas, and G. Uhlmann, *Anisotropic conductivities that cannot detected in EIT*, Physiol. Meas., 24 (2003), pp. 413–420.

[29] V. Grushin, *A certain class of hypoelliptic operators*, Mat. Sb., 83 (1970), pp. 456–473 (in Russian).

[30] B. Helffer and F. Nier, *Hypoelliptic estimates and spectral theory for Fokker-Planck operators and Witten Laplacians*, Lecture Notes in Math. 1862, Springer-Verlag, Berlin, 2005.

[31] T. Hoshina, K. Takizawa, J. Li, T. Kasama, H. Kakemoto, and T. Tsurumi, *Domain size effect on dielectric properties of barium titanate ceramics*, Jpn. J. Appl. Phys., 47 (2008), pp. 7607–7611.

[32] T. Kato, *Perturbation Theory for Linear Operators*, Springer-Verlag, Berlin, 1980.

[33] Y. Lai, J. Ng, H. Chen, D. Han, J. Xiao, Z. Zhang, and C. Chan, *Illusion optics: The optical transformation of an object into another object*, Phys. Rev. Lett., 102 (2009), 253902.

[34] M. Lassas and T. Zhou, *Two dimensional invisibility cloaking for Helmholtz equation and non-local boundary conditions*, Math. Res. Lett., 18 (2011), pp. 473–488.

[35] M. Lassas and T. Zhou, *The blow-up of electromagnetic fields in 3-dimensional invisibility cloaking for Maxwell's equations*, SIAM J. Appl. Math., 76 (2016), pp. 457–478.

[36] F. Lemoult, G. Lerosey, J. de Rosny, and M. Fink, *Resonant metalenses for breaking the diffraction barrier*, Phys. Rev. Lett., 104 (2010), 203901.

[37] S. Levendorskii, *Nonclassical spectral asymptotics*, Uspekhi Mat. Nauk, 43 (1988), 123 (in Russian); Russian Math. Surveys, 43 (1988), pp. 149–192 (in English).

[38] U. Leonhardt, *Optical conformal mapping*, Science, 312 (2006), pp. 1777–1780.

[39] U. Leonhardt and T. Tyc, *Superantenna made of transformation media*, New J. Phys., 10 (2008), 115026.

[40] R. Liu, C. Ji, J. J. Mock, and J. Y. Chin, *Broadband ground-plane cloak*, Science, 323 (2009), pp. 366–369.

[41] A. Menikoff and J. Sjöstrand, *On the eigenvalues of a class of hypoelliptic operators*, Math. Ann., 235 (1978), pp. 55–85.

[42] J. B. Pendry, D. Schurig, and D. R. Smith, *Controlling electromagnetic fields*, Science, 312 (2006), pp. 1780–1782.

[43] R. Montgomery, *A Tour of Subriemannian Geometries, Their Geodesics and Applications*, AMS, Providence, 2002.

[44] A. Nagel and E. M. Stein, *Lectures on Pseudodifferential Operators*, Princeton University Press, 1979.

[45] L. Rothschild and E. M. Stein, *Hypoelliptic differential operators and nilpotent groups*, Acta Math., 137 (1976), pp. 247–320.

[46] D. Schurig et al., *Metamaterial electromagnetic cloak at microwave frequencies*, Science, 314 (2006), pp. 977–980.

[47] C. Simovski, P. Belov, A. Atrashchenko, and Y. Kivshar, *Wire metamaterials: Physics and applications*, Adv. Mater., 24 (2012), pp. 4229–4248.

[48] R. Strichartz, *Sub-Riemannian geometry*, J. Differential Geom., 24 (1986), pp. 221–263.

[49] M. Taylor, *Partial Differential Equations*, II, Appl. Math. Sci. 116, Springer, 2006.

[50] A. Vshivzev, N. Norin, and V. Sorokin, *Solution of the spectral problem for the Schrödinger equation with a degenerate polynomial potential of even power*, Theoret. Math. Phys., 109 (1996), pp. 1329–1341.

[51] D. Werner and S. Ganguly, *An overview of fractal antenna engineering research*, IEEE Ant. Prop., 45 (2003), pp. 38–57.

[52] S. Zhang, D. Genov, C. Sun, and X. Zhang, *Cloaking of matter waves*, Phys. Rev. Lett. 100 (2008), 123002.